Journal of Power Sources 196 (2011) 7673–7680

Contents lists available at ScienceDirect

Journal of Power Sources

journal homepage: www.elsevier.com/locate/jpowsour

Diesel steam reforming with a nickel–alumina spinel catalyst for solid oxide fuel cell application

Clémence Fauteux-Lefebvre, Nicolas Abatzoglou*, Nadi Braidy, Ines Esma Achouri

Department of Chemical and Biotechnological Engineering, Université de Sherbrooke, Sherbrooke, Québec, Canada J1K 2R1

ARTICLE INFO

Article history:
Received 9 March 2011
Received in revised form 3 May 2011
Accepted 6 May 2011
Available online 17 May 2011

Keywords:
Steam reforming
Diesel
SOFC
Ni–alumina spinel
Catalyst

ABSTRACT

Liquid hydrocarbons (LC) are considered as fuel cells feed and, more particularly, as solid oxide fuel cell feed. Cost-effective LC-reforming catalysts are critically needed for the successful commercialization of such technologies. An alternative to noble metal catalysts, proposed by the authors in a previous publication, has been proven efficient for diesel steam reforming (SR). Nickel, less expensive and more readily available than noble metals, was used in a form that prevents deactivation. The catalyst formulation is a Ni–alumina spinel ($NiAl_2O_4$) supported on alumina (Al_2O_3) and yttria-stabilized zirconia (YSZ).

SR of commercial diesel was undertaken for more than 15 h at high gas hourly space velocities and steam-to-carbon ratios lower than 2. Constant diesel conversion and high hydrogen concentrations were obtained. Ni catalyst characterization revealed no detectable amounts of carbon on the spinel catalyst surface Ni. The effect of catalyst composition (Ni concentration and YSZ presence) was studied to understand and optimize the developed catalyst. Two phenomena were found to be influenced by relative catalyst composition: water–gas-shift vs reforming reaction extent, and concentration of light hydrocarbons in products.

1. Introduction

Solid oxide fuel cells (SOFCs) are an interesting alternative to the combustion engine to decrease world energy consumption and greenhouse gas emissions. Their thermodynamically calculated theoretical energy conversion efficiency is significantly higher than any other known engine. SOFC feed needs consist of as pure as possible H_2 and CO gaseous mixtures. Diesel steam reforming (DSR) to produce such mixtures for in-line SOFC feeding has considerable advantages: (1) it is safe since there is no hydrogen handling, (2) diesel volume density is high, and (3) the diesel distribution infrastructure and network already exist.

Hydrogen from diesel can be obtained from 3 different reactions: (1) steam reforming (SR) which is endothermic (Eq. (1)); (2) catalytic partial oxidation which is exothermic (Eq. (2)); combination of the above can be autothermal; (3) water gas shift (WGS) (Eq. (3)). Catalytic cracking has been tested as a step upstream of reforming by Campbell et al. [1], who reported a concentration of 10% hydrogen in products with conversion greater than 80%. In comparison, catalytic oxidation gives 35–45% molar hydrogen in products where as SR delivers 70–80% [2].

$$C_nH_m + nH_2O \rightarrow nCO + \left(n + \frac{m}{2}\right) H_2 \quad (1)$$

$$C_nH_m + \left(\frac{n}{2}\right) O_2 \rightarrow nCO + \left(\frac{m}{2}\right) H_2 \quad (2)$$

$$CO + H_2O \rightarrow CO_2 + H_2 \quad (3)$$

Catalyst deactivation is one of the most important issues in DSR. In addition to deactivation by coking and sintering, typical in reforming reactions, sulphur poisoning occurs from fossil diesel composition.

Coking is caused by 2 main reactions: (1) the Boudouard reaction, and (2) hydrocarbon decomposition (cracking) [3]. There are 3 types of coke formation in hydrocarbon-reforming reactions: encapsulated carbon, whisker carbon, and pyrolytic carbon [3]. Whisker carbon is formed after carbon dissolution into the metal catalyst. Pyrolytic carbon derives from hydrocarbon pyrolysis, which is typical of hydrocarbon chains. These 2 coking mechanisms are favoured at high temperatures employed in DSR. Commercial diesel is a variable mixture of liquid hydrocarbons (LC), including olefins, paraffin, cycloalkanes and aromatics. Its SR reaction kinetics depends on the chemical nature of the reformed molecules [4]. The prevailing mechanism (elementary reaction steps) is not yet well defined. However, various theoretical mechanisms have been proposed [5,6] with carbon formation on active sites being specific

* Corresponding author. Tel.: +1 819 821 7904; fax: +1 819 821 7955.
E-mail address: Nicolas.Abatzoglou@USherbrooke.ca (N. Abatzoglou).

0378-7753/$ – see front matter © 2011 Elsevier B.V. All rights reserved.
doi:10.1016/j.jpowsour.2011.05.003

steps of these mechanisms and depending on the reactants' water to carbon ratio (lower water to carbon ratio favour carbon formation on catalyst surface). In the case of LC, such as diesel, coking is also caused by the polymerization of heavy hydrocarbons [7].

Noble metal-based catalysts are more resistant than Ni to coking and their deactivation is, therefore, slower. The coking mechanism is different for Ni than for noble metals. Diffusion and dissolution of carbon into Ni causes catalyst breakage and eventually the formation of carbon whiskers due to local Ni saturation in carbon. Noble metals do not dissolve carbon to a significant extent, and they are, therefore, more resistant [4]. Ni catalysts are also more prone to coking owing to the fast dissociation of carbon–carbon bonds at the catalyst surface [8], leading to the accumulation of radical carbon species (CH_x; $x = 0$–3) at the surface and, therefore, to coke formation.

Ni catalysts are also prone to deactivation by sintering [9]. Catalyst preparation is known to influence metal dispersion at the surface of its support (usually ceramic); the higher the dispersion, the lower the sintering effect [10].

Sulphur contained in diesel is responsible for the formation of metal sulphides during catalytic reforming [11]. Catalytically active metal sites, thus, decrease directly with sulphides concentration. The catalyst becomes deactivated when a critically large percentage of sites are occupied. This sulphidation reaction has been found to be reversible at high temperatures in oxidizing atmosphere [12]. Sulphur is usually chemisorbed and forms sulphides; thus, poisoning is hardly reversible since regeneration results in specific surface loss. In addition to blocking active sites, sulphur modifies the catalyst surface [13]. Therefore, desulphurization steps are needed at high temperatures and under severe conditions, which can also impact the catalyst.

In research tests, noble metals have been shown to be more resistant to deactivation than Ni catalysts. Bimetallic catalysts often have a longer lifespan. In 1 case, bimetallic catalysts containing noble metals (Pd–Pt/CeO and Ni–Pt/CeO) were reported to be resistant in autothermic reforming of diesel (100 ppm sulphur) for 50 h while a mono-metallic catalyst (Pt/CeO) was deactivated within 30 h [14]. In another case, a bimetallic catalyst was compared to a Ni catalyst for SR of isooctane containing 500 ppm of sulphur. Activity of the bimetallic catalyst was maintained for 160 h, whereas the Ni catalyst was deactivated after 8 h [15].

Ni hexaaluminates $ANi_{0.4}Al_{11.6}O_{19-\delta}$ (A = Ba, La or Sr) have been tested for catalytic oxidation of pure *n*-tetradecane and *n*-tetradecane containing 50 ppm of sulphur. The catalyst was deactivated within 5.5 h with sulphur-free *n*-tetradecane and within 2 h with sulphur-containing *n*-tetradecane [16]. A lifespan of 53 h was reported for a Ni catalyst in sulphur-free hexadecane reforming, with a decrease in activity from 72% hydrogen in products to 65%, representing a 10% loss of activity [17].

In most research, the use of diesel surrogates rather than commercial diesel makes it difficult to compare the reported activities of different catalysts. Surrogates sometimes contain no sulphur or only 1 or 2 different hydrocarbons, which are not representative of real commercial diesel. Therefore, all reported catalysts (noble and non-noble metal-based) are deactivated within 100 h. In comparison, catalysts for methane SR have a lifespan of more than 5000 h [3] since a few decades. The efficiencies of different Ni catalysts have been demonstrated for methane and sulphur-free light hydrocarbon reforming. However, when these Ni-based catalysts were tested for sulphur-containing LC reforming, they were always rapidly deactivated.

Some authors have also observed that catalyst composition (including support composition and metal loading) has an impact on product concentrations in SR applications. Bellido and Assaf [18] demonstrated that the addition of Y_2O_3 or CaO to ZrO_2 support led to increased CO_2 and H_2 in products of ethanol reforming, due to the number of oxygen vacancies. Huang et al. [19] noted that the presence of Bi_2O_3 in Ni–Bi_2O_3/GDC catalyst helped to decrease CO production in methane reforming.

Ni spinel catalysts have been investigated for internal methane reforming in fuel cells, but the spinel was submitted to a partial reduction step prior to its use [20]. The catalyst was prepared by solid state reaction to form the spinel, followed by a reduction step to create a catalyst $(NiO)_x/Ni_{1-x}Al_2O_{4-x}$. Spinel stability at such conditions was studied by Jiong et al. [21]. He noted that spinel can give metallic Ni, but only at high severities.

In a previous publication [22], we developed a novel Ni–alumina spinel catalyst that was efficient and resistant for LC SR in its oxidized form. Conversions higher than 90% were obtained with products at equilibrium for hexadecane SR.

We propose this new spinel catalyst in commercial DSR. Its efficiency includes the absence of both significant deactivation by coking and observable sulphur poisoning. The effect of composition on reaction behaviour and product concentrations was studied.

2. Methodology

2.1. Catalyst preparation

Ni–alumina spinel catalysts on alumina and zirconia support were prepared according to the wet-impregnation method. Alumina powder (Al_2O_3, amorphous, average diameter of 40 μm from Alfa Aesar) and yttria-stabilized zirconia powder (YSZ:ZrO_2 with 7% Y_2O_3, average diameter size below 20 μm produced by plasma) were mixed together mechanically. Hexahydrate Ni nitrate ($Ni(NO_3)_2{\cdot}6H_2O$ from Alfa Aesar) served as Ni precursor. It was solubilized in water and added to the Al_2O_3/YSZ powder mixture with sufficient water to totally immerge the powder. The mixture was stirred for 90 min at room temperature, followed by a heating period of approximately 60 min at 95 °C to evaporate all the water. The impregnated sample was then dried overnight. The catalyst was heated at 900 °C for 6 h in the last preparation step. This enabled Ni nitrate to decompose into NiO and to react with part of the alumina support to form the spinel ($NiAl_2O_4$) – a solid state reaction. There was no subsequent preparation step (such as reduction) since the spinel was the targeted form. For spinel catalyst without zirconia, only alumina was used as support. Table 1 enumerates the different catalyst compositions.

05MeAlYSZ, a typical Ni catalyst for SR, was prepared for a control experiment, as per the same wet-impregnation method. The alumina support was α-phase (1 μm); the Ni precursor and the zirconia support were the same as for the spinel catalyst. The only methodological difference was that the catalyst was heated at 600 °C to form NiO and not at 900 °C as for the spinel. An additional step, catalyst reduction, was needed to form the metallic Ni catalyst, which was done at 500 °C for 1 h in 100% hydrogen atmosphere.

2.2. Catalyst characterization

Multipoint Brunauer Emmet and Teller (BET) surface area were measured using nitrogen adsorption using an Accelerated Surface Area and Porosimetry System (ASAP 2020) by Micromeritics'. Catalysts were examined by scanning electron microscopy (SEM) with an Hitachi S-4700 field emission gun and energy-dispersive X-ray spectroscopy (EDXS) with an Oxford EDXS detector and ultra-thin ATW2 window. Both fresh and used catalysts were subjected to Philips X'Pert Pro X-ray diffractometry (XRD), employing a monochromator with radiation Cu Kα1, 40 mA current and 45 kVs. Chemical surface analysis was completed by X-ray photoelectron spectroscopy (XPS) in an Axis Ultra DLD from Kratos Analytical Equipment with Al Kα monochromatic X-ray source. Calibration

Table 1
Formulation of different catalysts used in this study.

Catalyst	Ni content and form	Alumina type	Zirconia type	Calculated ratio Ni/Al_2O_3 (%)
05SpAlYSZ	5% – Spinel form ($NiAl_2O_4$)	γ – Amorphous, 40 μm	ZrO_2–Y_2O_3 (7%); <20 μm	10.53
05SpAl	5% – Spinel form ($NiAl_2O_4$)	γ – Amorphous, 40 μm	No	5.26
10SpAl	10% – Spinel form ($NiAl_2O_4$)	γ – Amorphous, 40 μm	No	11.10
2.5SpAl	2.5% – Spinel form ($NiAl_2O_4$)	γ – Amorphous, 40 μm	No	2.56
05MeAlYSZ	5% – Metallic Ni	α, 1 μm	ZrO_2–Y_2O_3 (7%); <20 μm	10.53

of the curve due to charge was based on the binding energy (BE) of the adventitious carbon (BE = 285 eV) [23] (contaminant carbon).

2.3. Reforming experiments

Details of the experimental set-up are provided in a previous publication [22], but necessary information is given below: the reactor's inner diameter was 46 mm, and catalytic bed length was 60 mm. The powder catalyst was dispersed in quartz wool, and compacted in the reactor to form a catalytic bed.

An emulsion-in-water technique was adopted for diesel injection. This method was chosen to enhance hydrocarbon/water mixing. The 2 immiscible reactants were emulsified according to a surfactant-aided protocol. The reactants entered at room temperature, were heated rapidly and vaporized in the pre-heating zone maintained at 550 °C. Argon served as inert diluent, carrier gas and internal standard for LC SR.

The axial variation of temperature was measured using a thermocouple placed at the center and able to move along the cylindrical reactor axis. Measurements were taken at every 5 cm from the top of the reactor down to the reaction zone. The indicated reaction temperature is the one taken at the center of the reaction zone. The temperature upstream the catalyst bed was between 30 °C and 45 °C below the reaction temperature, depending on the operating parameters. The radial profile of the temperature in the reaction zone was also measured; there is a 25 °C gradient between the reactor wall and the bed center. The reported reaction temperature is the one at the center of the reactor near the bottom of the reaction zone. This is considered as being representative of the reaction zone because it is equal to the mathematically calculated average temperature based on the axial and radial profiles reported above.

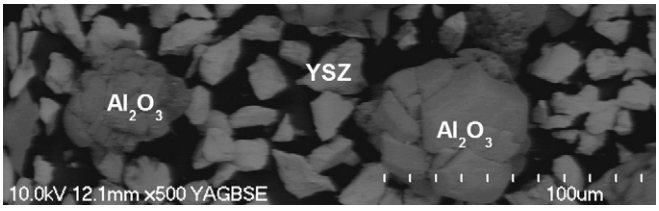

Fig. 1. SEM micrograph of impregnated support for spinel catalyst 05SpAlYSZ.

Table 2
Details of GC measurement errors including concentration of external standard.

Gas	Standard gaseous concentration (%)	Absolute error (on% concentration of the standard)	Relative error (%)
H_2	55.16	0.46	0.83
CO	19.70	0.21	1.05
CO_2	6.96	0.38	5.45
CH_4	2.08	0.04	1.87
Ar	16.10	0.22	1.37

Various temperatures and gas hourly space velocities (GHSV) were applied in the DSR tests. In all cases, the water to carbon molar ratio was 1.9. Reforming products were analyzed by Varian CP-3800 gas chromatography (GC). The exit gaseous flow rate was measured by a flow rate mass meter (Omega FMA-700A) calibrated for nitrogen. Since it is a mixture, the flow rate was calculated using conversion factors based on thermal conductivities of each gas and their concentrations obtained by the GC analysis. Ultra-low sulphur-containing diesel (<15 ppm) was purchased at an Olco gas station in Sherbrooke (Quebec, Canada – July 2008). Experimental conversion was calculated according to Eq. (4):

$$X = \frac{N_{CO_{out}} + N_{CO_2} + N_{CH_4}}{N_{C_mH_n} \times m + N_{Surfactant_{in}} \times Y} \quad (4)$$

with N_i being the total number of moles of component i (i = CO, CO_2, CH_4) at the reactor exit or inlet, and Y being the number of carbon

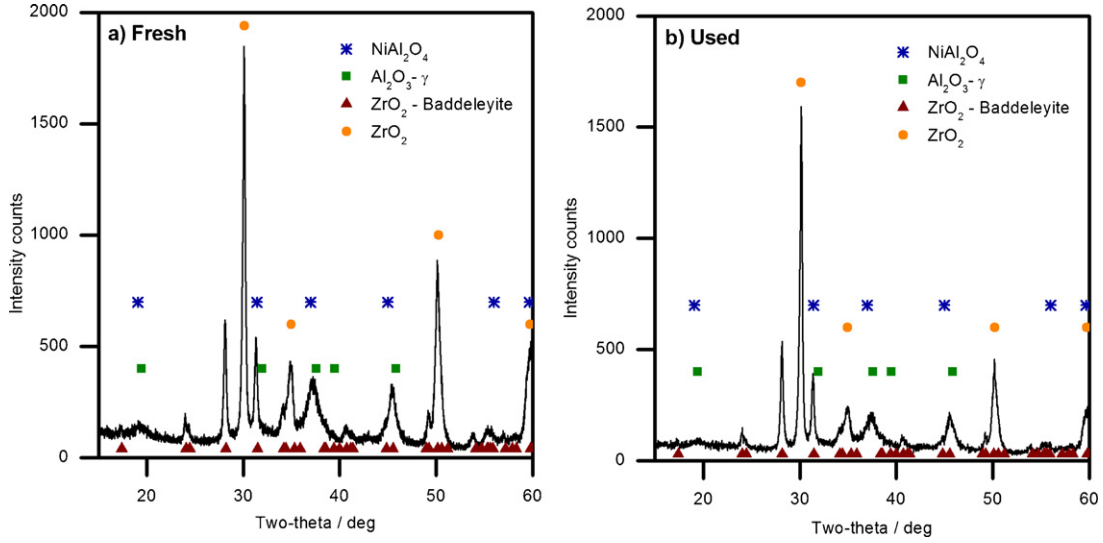

Fig. 2. XRD analysis of spinel catalyst 05SpAlYSZ: (a) fresh catalyst and (b) used catalyst in DSR at 4600 $cm^3\ g^{-1}\ h^{-1}$; T = 710 °C.

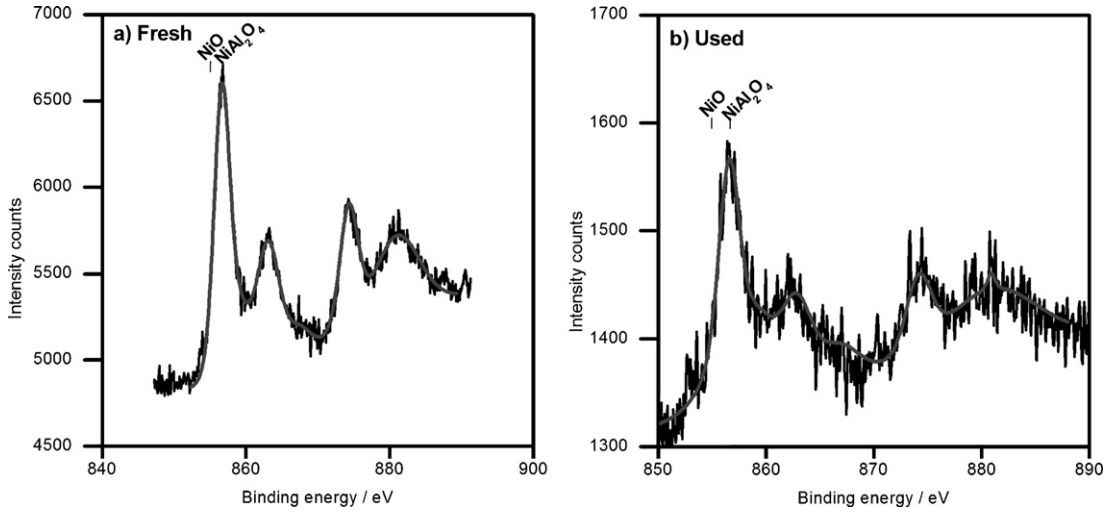

Fig. 3. XPS analysis of spinel catalyst 05SpAlYSZ: (a) fresh catalyst and (b) used catalyst in DSR at 25,000 $cm^3\ g^{-1}\ h^{-1}$; $T = 700\ ^\circ C$.

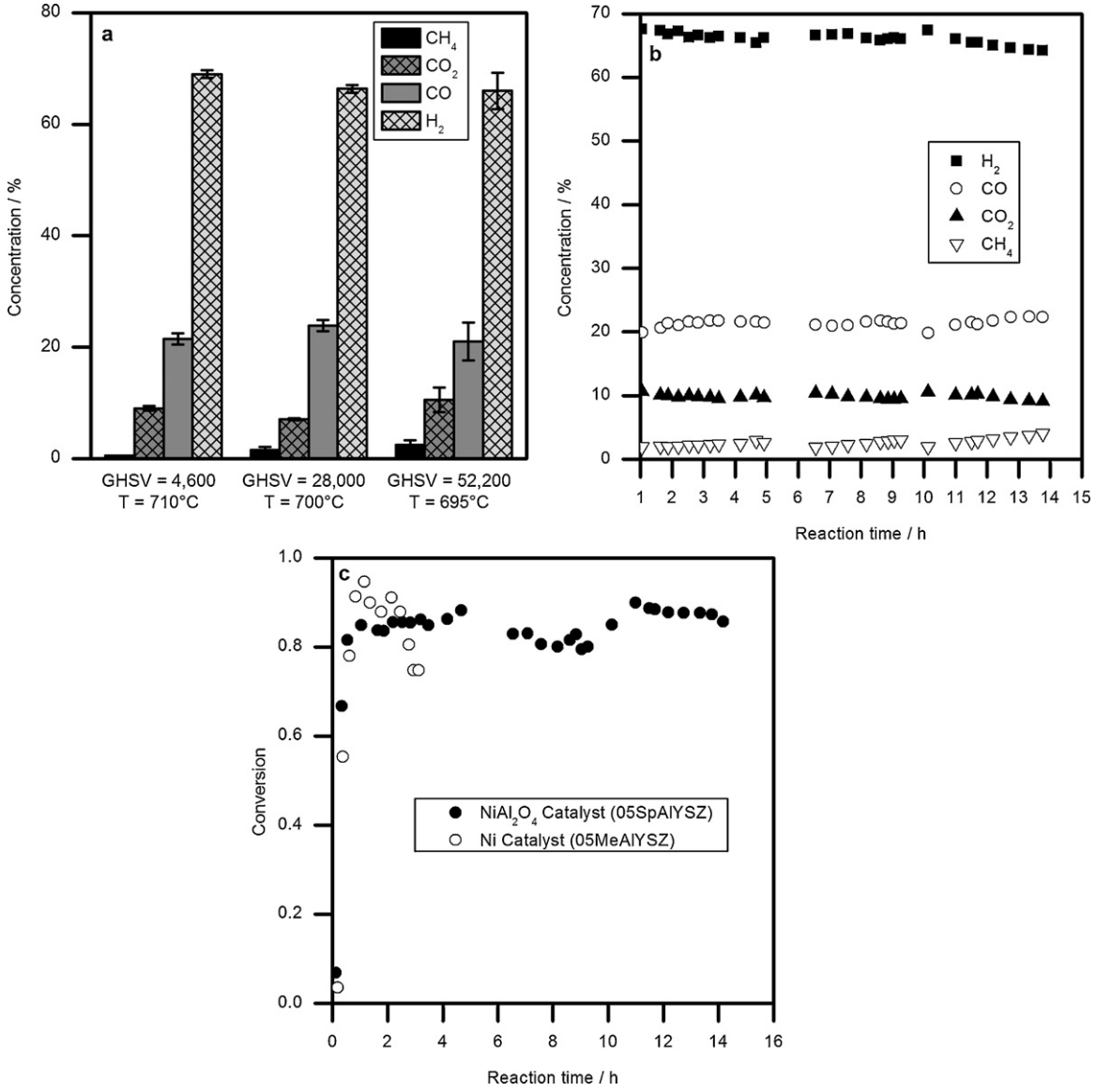

Fig. 4. DSR experiments: (a) catalyst 05SpAlYSZ at different operating conditions (GHSV in $cm^3\ g^{-1}\ h^{-1}$), (b) long-term experiment with catalyst 05SpAlYSZ, and (c) comparison between metallic nickel catalyst 05MeAlYSZ and spinel catalyst 05SpAlYSZ.

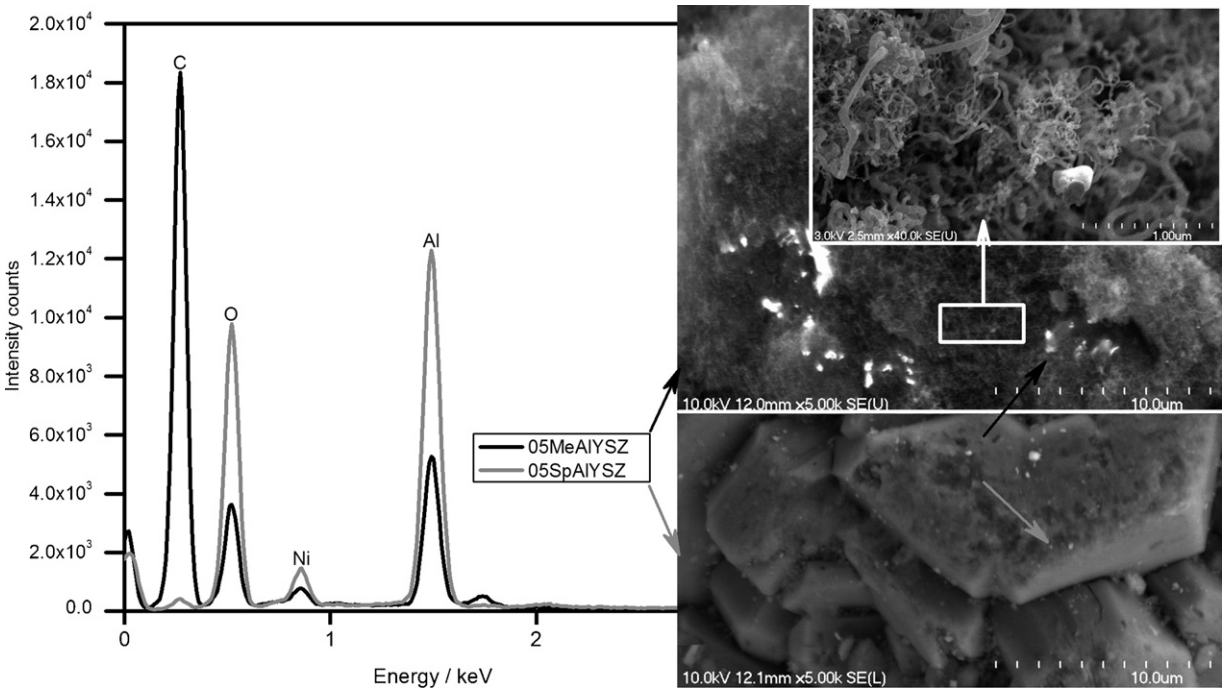

Fig. 5. SEM–EDXS analysis of spinel catalyst 05SpALYSZ and metallic nickel catalyst 05MeAlYSZ after use in DSR experiments.

atoms in the surfactant. Overall conversion was calculated for LC reforming based on the total amount of carbon fed in the reactor. Hydrocarbons were deemed to be converted when they were transformed into gaseous products (CO, CO_2 or CH_4). Carbon found in the reactor after the experiment was, therefore, not considered as converted hydrocarbon.

To calculate conversion, a LECO SC632 equipment quantified the amount of carbon in the reactants after calibration with dodecane (84.7%). In addition, diesel saturation level was evaluated by the Wijs test [24].

Reactor exit concentrations of H_2, CO, CO_2 and CH_4 in the tests reported were compared to theoretical thermodynamic equilibrium concentrations, to determine if equilibrium was reached. Thermodynamic equilibrium concentrations were calculated with FactSage software on the basis of Gibbs energy minimization [25].

3. Results and discussion

3.1. Catalyst characterization

All surface analyses of fresh catalyst were performed with a 05SpAlYSZsample. Fig. 1 clearly shows that alumina and zirconia particles did not form a single solid phase because the 2 powders were prepared by impregnation. It has been demonstrated [22] that Ni is exclusively associated with alumina particles for this catalyst. There was no detectable amount of Ni on zirconia; therefore, Ni could be transformed into its Ni–alumina spinel form if the combination kinetics/duration of heat treatment allows for it.

The route to build $NiAl_2O_4$ in the catalyst included a NiO formation step, as shown in (5) and (6).

$$x\mathrm{Ni(NO_3)_2{\bullet}6H_2O} + y\mathrm{Al_2O_3} \rightarrow x\mathrm{NiO} + y\mathrm{Al_2O_3} + \mathrm{gas} \quad (5)$$

$$x\mathrm{NiO} + y\mathrm{Al_2O_3} \rightarrow x\mathrm{NiAl_2O_4} + (y-x)\mathrm{Al_2O_3} \quad (6)$$

It was, thus, important to ensure that step (5) was well completed. Two simple tests were conducted to rule out the existence of NiO. First, NiO is green, whereas this catalyst gives a blue tint to the white Al_2O_3/YSZ mixture, which is typical of $NiAl_2O_4$. Second, the catalyst was resistant to chlorhydric (HCl) and nitric (HNO_3) acid solutions while NiO was completely digested (dissolved) by these strong acids.

The presence of the spinel $NiAl_2O_4$ and the absence of NiO was confirmed by two analysis: XRD and XPS. Fig. 2 presents the XRD pattern. Fig. 2a reports the results of analysis before use, with Fig. 2b divulging data after use, as discussed in Section 3.2. The pattern was apparently dominated by YSZ. No NiO peaks were present in both analyses, indicating no NiO remaining in the fresh catalyst or NiO formation during the reaction. The other interesting features of XRD spectra included weak and broad peaks likely assigned to the mixture of low crystallinity γ-Al_2O_3. γ-Al_2O_3 and $NiAl_2O_4$ both shared the same Bravais lattice with similar lattice parameters, making them difficult to differentiate, especially when the diffraction lines were broadened.

$NiAl_2O_4$ formation was confirmed by analysis of Ni L_{23} edges with XPS of the catalyst formulation (Fig. 3a). The main features (L_3 peak position, L_2–L_3 energy separation, satellite peak position) were consistent with typical Ni L_{23} edges associated with $NiAl_2O_4$ [26,27]. Ni 2p3/2 position was 856.7 eV which corresponded to binding energy Ni 2p3/2 reported for $NiAl_2O_4$ [27]. It should also be noted that the position of the Ni 2p3/2 peak for NiO was found at typically lower binding energy (around 855 eV [26]), once again confirming the absence of NiO formation from the spinel catalyst. Fig. 3b presents the results of analysis after use and is shown here for comparison but discussed in Section 3.2.

3.2. Diesel steam reforming

In accordance with Canadian regulations [28], the maximum sulphur concentration is 15 mg kg^{-1} of diesel. The quantity of carbon in diesel measured with the LECO was 90.6%. Wijs analysis disclosed that diesel contained 0.98% of carbons in double bonds. An average molecular composition of $C_{12}H_{20}$ was calculated on the basis of these 2 measurements to estimate GHSV. Finally, Table 2 enumerates the GC measurement errors for each product analyzed in the DSR experiments. An external standard having gaseous con-

Table 3
Comparison of catalysts used for DSR.

Run	Time on stream	GHSV ($cm^3\ g^{-1}\ h^{-1}$)	Temp (°C)	Catalyst	BET area of fresh catalyst ($m^2\ g^{-1}$)	BET area of used catalyst ($m^2\ g^{-1}$)	Conversion (± 3%) (%)
1	5	4600	710	05SpAlYSZ	39	64	85
2	15	52,200	695	05SpAlYSZ	39	34	85
3	3	43,400	705	05MeAlYSZ	8	29	73

centrations similar to those of reforming experiment was used to evaluate the GC measurement errors.

Fig. 4a lists the dry gas concentration of reaction products for DSR with the Ni–alumina spinel catalyst 05SpAlYSZ in 3 different sets of operating conditions. The graph shows that with this catalyst a high hydrogen concentration can be obtained from DSR. The hydrogen concentrations were between 66% and 69% depending of the operating conditions while the theoretical equilibrium concentration of hydrogen for DSR is between 65% and 70%; the exact value cannot be estimated, commercial diesel being a complex mixture as already mentioned. For the three sets of operating conditions, the reaction was close to the theoretical thermodynamic equilibrium. The only significant difference was in the CO/CO_2 ratio which was attributed to somehow slower WGS kinetics.

Fig. 4b depicts dry gas concentrations of the reaction products overtime, showing that reactor outlet concentrations were essen-

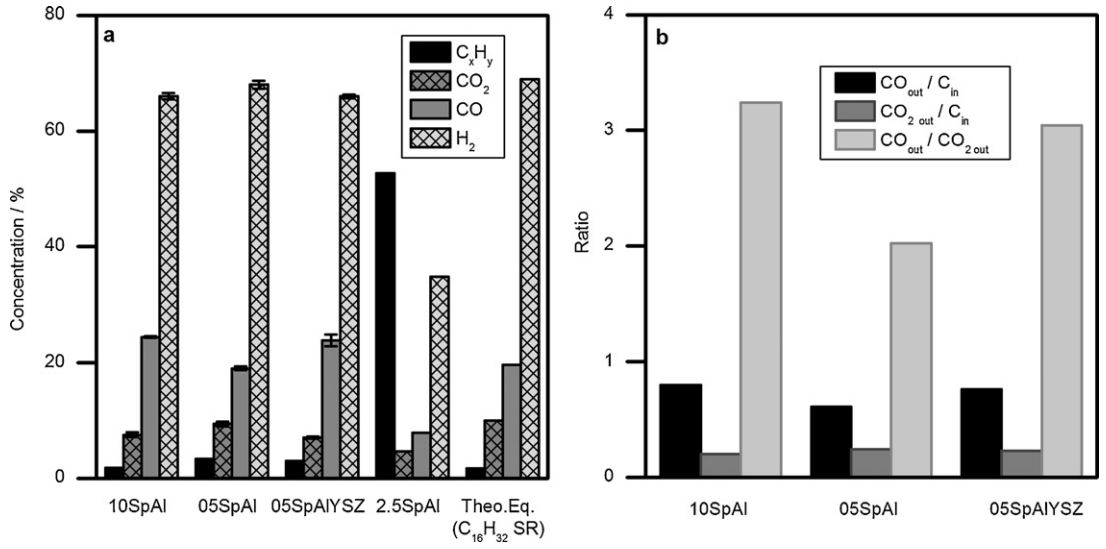

Fig. 6. Effect of catalyst composition in DSR experiments (catalysts 10SpAl, 05SpAl, 05SpAlYSZ, GHSV = 25,000 $cm^3\ g^{-1}\ h^{-1}$, T = 700 °C): (a) average product concentrations at the exit of reactor and (b) ratio of carbon monoxide and carbon dioxide in products.

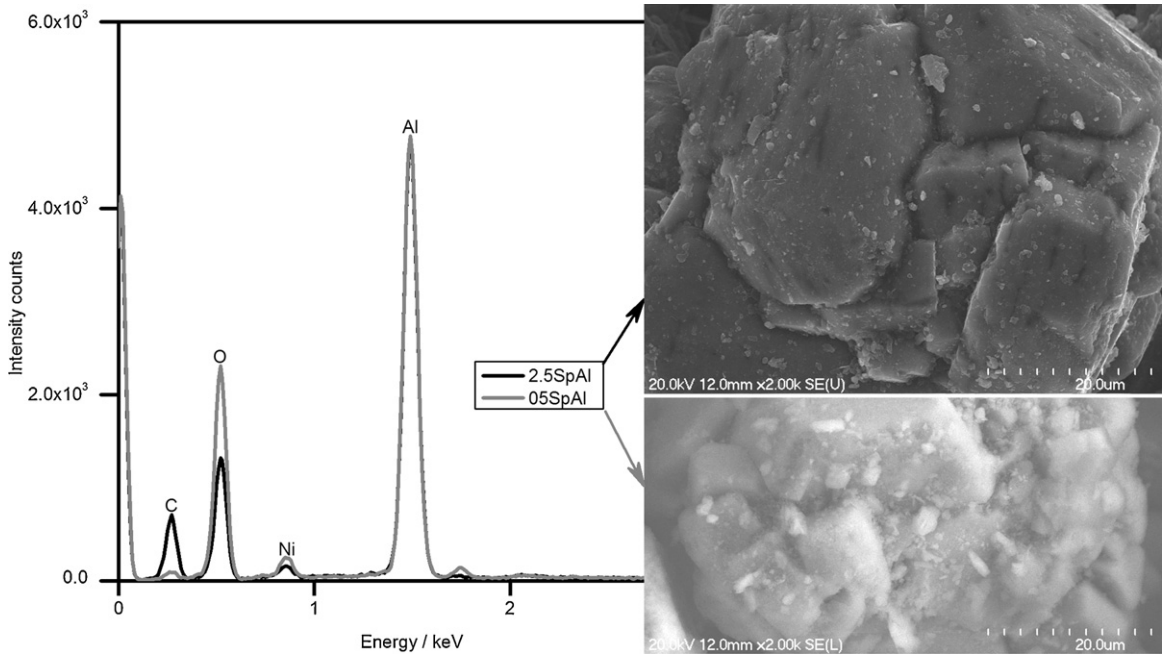

Fig. 7. SEM–EDXS analysis of spinel catalyst 05SpAl with different nickel concentrations (05SpAl and 2.5SpAl) after use in DSR experiments.

tially stable over 15 h, with a high GHSV of 52,200 $cm^3\ g^{-1}\ h^{-1}$ and a low steam to carbon molar ratio. As indicated in Section 1, a low steam to carbon ratio favours the coking mechanisms and nickel catalysts are usually deactivated within 10 h. In the case of the spinel Ni–alumina catalyst, there was no significant decrease in hydrogen concentration or increase in methane concentration that would indicate severe catalyst deactivation after 15 h, and the overall conversion was 85%. This high conversion and the concentration of hydrogen near of the equilibrium indicate a high yield in hydrogen in the products.

Fig. 4c compares catalyst 05SpAlYSZ (spinel) and catalyst 05MeAlYSZ (metallic) for conversion vs time in similar operating conditions (spinel catalyst: GHSV = 52,200 $cm^3\ g^{-1}\ h^{-1}$, T = 695 °C; metallic catalyst: GHSV = 43,400 $cm^3\ g^{-1}\ h^{-1}$, T = 705 °C). It clearly shows the higher lifespan of the spinel catalyst over a typical Ni catalyst which was deactivated after 3 h. It can be observed that conversion was slightly higher for the metallic Ni catalyst at the beginning of the reaction. However, deactivation of the metallic catalyst was fast, and conversion became lower than that of the spinel after only 2 h.

This experiment was stopped because the formed coke, linked to catalyst deactivation, blocked the reactor exit and increased reactor pressure prohibitively. Global conversion after 3 h was only 73%, at a 17% lower gas velocity than that used with the spinel catalyst.

Fig. 5c compares catalysts 05SpAlYSZ and 05MeAlYSZ in DSR experiments by SEM–EDXS analysis. No carbon was apparent under SEM or detected by EDXS on the Ni–alumina spinel catalyst after 15 h in the DSR test. In comparison, whisker carbon formation from coking was observed on the metallic Ni catalyst in the 3-h DSR test. Table 3 reports conversions and BET surface areas before and after the experiments.

A difference was noted in specific area of the spinel and metallic catalysts. However, deactivation was not attributed to this difference; the effect was rather observed on activity. An increase in catalyst area was evident in the experiment at GHSV of 4600 $cm^3\ g^{-1}\ h^{-1}$ with the spinel catalyst, which was expected because of catalyst attrition. In all cases, no severe sintering was observed.

XRD (Fig. 2b) is the analysis of the spinel catalyst 05SpAlYSZ used for SR run 1 and XPS (Fig. 3b) is the analysis of the spinel catalyst 05SpAlYSZ used for SR run 3. The only significant phase after the reforming experiments is the $NiAl_2O_4$. The XRD reveals no Ni or NiO and the dominant pic observed by XPS is associated with the spinel phase ($NiAl_2O_4$). As for the fresh catalyst, the position of the principal peak for Ni 2p3/2 and the doublet separation are characteristic of the spinel. These two analyses indicate that there was no reduction of the catalyst due to hydrogen produced by the SR reaction. The low signal of the XPS after use is attributed to a thin carbon layer deposition that had not observable effects on catalytic properties.

The spinel catalyst was demonstrated to be active for DSR. As mentioned, high conversions with short residence times were obtained with a low steam to carbon ratio. Compared to the metallic Ni catalyst, performance was higher with longer lifespan and higher conversion. The most important point was that the catalyst was not deactivated by coking and no carbon was found on the surface. In addition, sulphur poisoning was not seen for the duration of reaction time, even if fossil diesel was used.

3.3. Effect of Ni–alumina spinel catalyst composition

DSR experiments were conducted at different compositions to analyze the effect of catalyst composition. The outcome of YSZ presence in the support was studied since there was particulate segregation and no Ni on the zirconia support. The influence of Ni concentration was investigated as well. Experiments were performed at GHSV of 25,000 $cm^3\ g^{-1}\ h^{-1}$ and temperature of 700 °C. The following catalysts were tested: 05SpAlYSZ, 10SpAl, 05SpAl and 2.5SpAl.

The effects of Ni–alumina catalyst composition in DSR were assessed, with Fig. 6a showing that it had an impact on product concentrations, including the quantity of hydrocarbons. Conversions were higher than 90% with catalysts containing 5% and 10% (w/w) Ni. However, conversion with the catalyst holding 2.5% (w/w) Ni was less than 25%, mainly because of thermal cracking and not reforming. The catalyst with a 2.5% Ni load was not active for catalytic reforming, while at 5% Ni load the conversion due to steam reforming was higher than 90%. This indicates that at the tested experimental conditions there is a breaking point between 2.5% and 5% Ni load.

In Fig. 6b, it can be seen that increasing Ni concentration from 5% to 10% and modifying support composition had a significant effect on relative product concentrations, but not on overall conversion. It had an influence on WGS reaction extent. The results with zirconia for a 5% Ni load catalyst were similar to those with 10% Ni load and alumina. These 2 catalysts (05SpAlYSZ and 10SpAl) had the same Ni to alumina ratio. The only observed difference was in hydrocarbons concentration, but the latter was of the same order of magnitude with the experimental error. For both catalysts above, CO_2 is lower than predicted by equilibrium; this means that WGS reaction extent is lower. The catalyst 05SpAl gave concentrations closer to those predicted by equilibrium calculations.

Fig. 7 reports the results of SEM–EDXS analysis and compares catalysts with 2.5% and 5% Ni (catalysts 055SpAl and 2.5SpAl, respectively) after the DSR experiment. It shows that even if the 2.5% Ni spinel catalyst was not active, there was no carbon formation from coking. Even if there was a minimum concentration of Ni necessary for the catalyst, when the Ni concentration was sufficient (5%), the catalyst was efficient for DSR with high conversion. No coking or sulphur poisoning was observed by EDSX or XPS on the spinel catalyst after DSR, even with no activity throughout the duration of the experiment (2.5% Ni content).

4. Conclusion

An Al_2O_3/YSZ-supported $NiAl_2O_4$ catalyst was tested efficiently in DSR. Its molecular composition was confirmed by XPS, XRD, SEM and other complementary techniques. Our study demonstrated that the Ni-based catalyst (non-noble metal) in its spinel form was effective for DSR with no deactivation for more than 15 h at high GHSV. No significant coking occurred on the catalyst surface after the experiment, while a Ni catalyst under similar conditions was deactivated because of severe whisker coke formation. No sulphur poisoning was observed at this point.

In addition, our data demonstrated that catalyst formulation (support as well as the amount of Ni) had an important effect on WGS reaction extent and complete hydrocarbon conversion. The Ni to alumina ratio seems to be an important factor in catalyst composition, while YSZ presence, in this specific catalyst form and under the tested experimental conditions, did not show a significant influence on the catalytic performance. Furthermore, the catalyst containing 2.5% Ni in spinel form was not effective for DSR, but coking extent was insignificant.

Acknowledgements

The authors are indebted to SOFC (Solid Oxide Fuel Cells) Network Canada for funding of this project. The financial contributions of the Natural Sciences and Engineering Research Council of Canada (NSERC) through Discovery Funding and Student Awards is also

acknowledged along with student awards from Fonds québécois de la recherche sur la nature et les technologies (FQRNT). Many thanks are due to Henri Gauvin for technical support, to Sonia Blais and Stéphane Gutierrez for catalyst characterization, and to Carmina Reyes Plascencia for Wijs analysis. Finally, special thanks to Ovid Da Silva for thorough reading of the manuscript.

References

[1] T.J. Campbell, A.H. Shaaban, F.H. Holcomb, R. Salavani, M.J. Binder, J. Power Sources 129 (2004) 81–89.
[2] A.F. Ibarreta, C. Sung, Int. J. Hydrogen Energy 31 (2006) 1066–1078.
[3] J.R. Rostrup-Nielsen, in: J.R. Anderson, M. Boudart (Eds.), Catalysis, Science and Engineering, vol. 5, second ed., Springer, Berlin, 1984, pp. 1–130.
[4] M.C. Alvarez-Galvan, R.M. Navarro, F. Rosa, Y. Briceno, F. Gordillo Alvarez, J.L.G. Fierro, Int. J. Hydrogen Energy 33 (2008) 652–663.
[5] J.R. Rostrup-Nielsen, J. Sehested, Stud. Surf. Sci. Catal. 139 (2001) 1–12.
[6] F. Melo, N. Morlanes, Catal. Today 133–135 (2008) 374–382.
[7] B.D. Gould, A.R. Tadd, J.W. Schwank, J. Power Sources 164 (2007) 344–350.
[8] E. Nikolla, A. Holewinski, J. Schwank, S. Linic, J. Am. Chem. Soc. 128 (2006) 11354–11355.
[9] A.P.E. York, T. Xiao, M.L.H. Green, J.B. Claridge, Catal. Rev. – Sci. Eng. 49 (2007) 511–560.
[10] L. Oukacine, F. Gitzhofer, N. Abatzoglou, D. Gravelle, Surf. Coat. Technol. 201 (2006) 2046–2053.
[11] R.M. Navarro, M.A. Pena, J.L.G. Fierro, Chem. Rev. 107 (2007) 3952–3991.
[12] A. Azad, M.J. Duran, Appl. Catal. A 330 (2007) 77–88.
[13] C.H. Bartholomew, Appl. Catal. A 212 (2001) 17–60.
[14] P.K. Cheekatamarla, A.M. Lane, Int. J. Hydrogen Energy 30 (2005) 1277–1285.
[15] Q. Ming, T. Healey, L. Allen, P. Irving, Catal. Today 77 (2002) 51–64.
[16] T.H. Gardner, D. Shekhawat, D.A. Berry, M.W. Smith, M. Salazar, E.L. Kugler, Appl. Catal. A 323 (2007) 1–8.
[17] D.H. Kim, J.S. Kang, Y.J. Lee, N.K. Park, Y.C. Kim, S.I. Hong, D.J. Moon, Catal. Today 136 (2008) 228–234.
[18] J.D.A. Bellido, E.M. Assaf, J. Power Sources 177 (2008) 24–32.
[19] T.-J. Huang, M.-C. Huang, M.-S. Huang, Appl. Catal. A 354 (2009) 127–131.
[20] L. Kou, J.R. Selman, J. Appl. Electrochem. 30 (2000) 1433–1437.
[21] Y.S. Jiong, L. Kou, P. Nash, J.R. Selman, Proceedings of the Fourth International Symposium on Carbonate Fuel Cell Technology, 1997, pp. 456–468.
[22] C. Fauteux-Lefebvre, N. Abatzoglou, J. Blanchard, F. Gitzhofer, J. Power Sources 195 (2010) 3275–3283.
[23] X-ray Photoelectron Spectroscopy (XPS) Reference Pages, Analytical Services – Surface Sciences Western – University of Western Ontario, Canada.
[24] AOCS Official Method Ja 14-91 for Iodine Value.
[25] C.W. Bale, P. Chartrand, S.A. Degterov, G. Eriksson, K. Hack, R. Ben Mahfoud, J. Melançon, A.D. Pelton, S. Petersen, CALPHAD: Comput. Coupling Phase Diagrams Thermochem. 26 (2002) 189–228.
[26] M.E. Rivas, J.L.G. Fierro, R. Guil-López, M.A. Peña, V. La Parola, M.R. Goldwasser, Catal. Today 133–135 (2008) 367–373.
[27] T. Osaki, T. Mori, J. Non-Cryst. Solids 355 (2009) 1590–1596.
[28] Canadian Environmental Protection Act, Sulphur in Diesel Fuel Regulations, SOR/2002-254, 2003.